# Study on the Frost Heave Damage Mechanism and Performance Degradation of Concrete Components in Slab Track Structures in Cold Regions

**Abstract:** This study investigates the frost heave-induced damage mechanism and performance degradation of concrete components in CRTS I slab track systems in cold regions. A 3D finite element model was developed based on plastic damage mechanics theory and the GB 50010-2010 Code for Design of Concrete Structures, systematically analyzing the effects of frost heave wavelength, amplitude, and location on damage evolution in the base plate and track slab. Key findings include: (1) Damage sequence discrepancy: The base plate enters a significant damage stage (damage factor = 0.25) at 8.5 mm frost heave amplitude, whereas the track slab exhibits abrupt damage (damage factor = 0.819) only at 13 mm, highlighting the base plate's higher susceptibility due to lower strength. (2) Failure mode contrast: The base plate shows compressive softening (post-peak stress drop), while the track slab demonstrates tensile ductility with sustained high residual stress post-cracking. (3) Frost heave parameter effects: Shorter wavelengths (10 m) and higher amplitudes (>8 mm) exacerbate damage. When the frost heave peak shifts from the base plate center to the track slab center, damage energy increases by 18%–20.5%. The results provide theoretical support for optimizing CRTS I track design and maintenance, recommending prioritized base plate crushing prevention (≥8 mm amplitude) and long-term monitoring of track slab tensile cracks (≥13 mm).

***Keywords*:** CRTS I slab track; cold regions; frost heave; plastic damage; finite element modeling; damage evolution; performance degradation

## 0 Introduction

With the continuous expansion of China's high-speed railway network into cold regions, the long-term service performance of ballastless track systems under frost heave in seasonally frozen ground has become an increasingly prominent issue. Frost heave-induced subgrade deformation can lead to interlayer separation within the track structure, damage to concrete components, and track geometry irregularities, all of which pose critical risks to train operation safety and passenger comfort [1]. Among various track systems, the CRTS I slab track has seen widespread application in cold regions due to its structural stability and high construction efficiency. However, compared to the CRTS III slab track, the differential damage mechanisms of the base plate and track slab under repeated frost heave cycles in CRTS I structures have not been systematically investigated. Most existing studies adopt linear elastic analysis methods [2], which are insufficient to accurately capture the cumulative plastic damage behavior of concrete under frost conditions. Wang et al. [3], through frost heave–load coupling experiments, demonstrated the significance of employing an elasto-plastic constitutive model for concrete to simulate frost-induced damage behavior.

In recent years, research on the response mechanisms of ballastless tracks under frost heave environments has gradually deepened. Wang et al. [4] proposed a damage-plasticity model incorporating reinforcement effects for CRTS III slab tracks, thoroughly analyzing the

effects of various frost heave parameters on structural deformation, interlayer separation, and stress–damage evolution. Zeng [5] established a thermal field model of a bridge-mounted CRTS I twin-block ballastless track using finite element software, investigating the mechanical performance under thermal loads, the variation in temperature-induced stresses in the track slab across different schemes, and the roles of diagonal reinforcement and expansion joints. Song [6] developed a thermo-mechanical coupling analysis method for CRTS III slab tracks by integrating temperature and train loads.

This study develops a three-dimensional finite element model of the CRTS I slab track–subgrade system based on plastic damage mechanics theory and the concrete constitutive model specified in the *Code for Design of Concrete Structures (GB 50010-2010)* [7]. It systematically investigates the spatiotemporal evolution of damage in the base plate and track slab under frost heave loading. By introducing parameterized frost heave scenarios, the performance degradation characteristics of C40 and C60 concrete during the three-stage damage process—elastic response, microcrack initiation, and macro-scale failure—are comparatively analyzed. The findings provide theoretical and engineering insights to support the optimized design, maintenance strategy development, and repair technologies of CRTS I slab track structures in severe cold regions.

## 1. Theoretical Verification

### 1.1 *Validation of the Concrete Plastic Damage Constitutive Model*

The concrete plastic damage model introduces stiffness degradation factors to describe the deterioration behavior of concrete under tensile and compressive stress states. This model assumes that concrete failure results primarily from two mechanisms—tensile cracking and compressive crushing—which are coupled within a unified theoretical framework.

In this theory, the nonlinear response of the material mainly arises from the interaction between plastic strain and damage variables, allowing accurate characterization of the damage evolution behavior of concrete under various loading paths. Numerical simulations of uniaxial tension and compression behavior demonstrate that the model can effectively reproduce the complete process of crack initiation, propagation, and final failure. The corresponding stress–strain curves of concrete under these two loading conditions are shown in Figure 1.

When concrete enters the softening phase of its stress–strain response under load and subsequently unloads, the material stiffness does not recover to its initial value, indicating irreversible degradation behavior. This degradation is primarily attributed to microcrack development and cumulative damage, and it is commonly characterized using a tensile damage factor and a compressive damage factor. Based on this concept, the concrete plastic damage model couples material damage behavior with plastic strain, and its constitutive relation can be expressed in the following form:

$$\sigma_t = (1-d_t)E_0\left(\varepsilon_t - \tilde{\varepsilon}_t^{pl}\right) \tag{1}$$

$$\sigma_c = (1-d_c)E_0\left(\varepsilon_c - \tilde{\varepsilon}_c^{pl}\right) \tag{2}$$

Here, the subscripts *t* and *c* denote the mechanical behavior of concrete under tension

and compression, respectively; $\tilde{\varepsilon}_t^{pl}$ and $\tilde{\varepsilon}_c^{pl}$ represent the equivalent plastic strains in tension and compression; $E_0$ is the initial elastic modulus of the concrete material prior to the onset of damage.

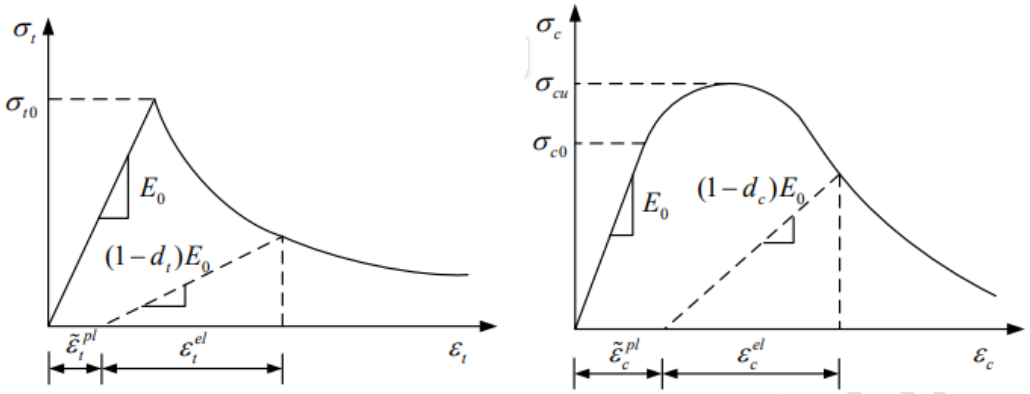


(a) Uniaxial tension (b) Uniaxial compression

**Fig .1 Uniaxial mechanical behavior of concrete**

In the Concrete Damaged Plasticity (CDP) model of ABAQUS, it is necessary to define two key parameter relationships: the tensile damage factor versus inelastic strain, and the compressive damage factor versus inelastic strain. Figures 2(a) and 2(b) show the stress–strain curves of concrete under uniaxial compression and uniaxial tension, respectively.

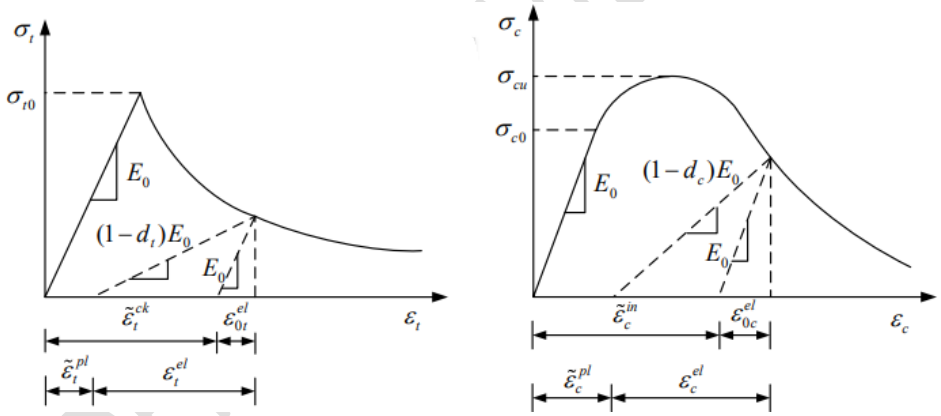


(a) Uniaxial tensile stress–strain curve (b) Uniaxial compressive stress–strain curve

**Fig .2 Stress–strain relationships of concrete in the plastic damage model**

As shown in Fig. 2, concrete exhibits linear elastic behavior under uniaxial tension (or compression) before reaching the peak stress. Beyond this point, it enters a softening stage accompanied by progressive stiffness degradation. The tensile inelastic strain $\tilde{\varepsilon}_t^{ck}$ and compressive inelastic strain $\varepsilon_{0c}^{el}$ are defined as follows:

$$\tilde{\varepsilon}_t^{ck} = \varepsilon_t - \varepsilon_{0t}^{el} = \varepsilon_t - \frac{\sigma_t}{E_0} \tag{3}$$

$$\tilde{\varepsilon}_c^{in} = \varepsilon_c - \varepsilon_{0c}^{el} = \varepsilon_c - \frac{\sigma_c}{E_0} \tag{4}$$

Substituting Equations (3) and (4) into the constitutive relationships of the concrete plastic damage model, i.e., Equations (1) and (2), yields the relationships between the tensile equivalent plastic strain $\varepsilon_t^{pl}$ and the tensile inelastic strain $\varepsilon_t^{ck}$, as well as between the compressive equivalent plastic strain $\varepsilon_c^{pl}$ and the compressive inelastic strain $\varepsilon_c^{in}$, as shown below:

$$\varepsilon_t^{pl} = \varepsilon_t^{ck} - \frac{d_t}{(1-d_t)}\frac{\sigma_t}{E_0} \tag{5}$$

$$\varepsilon_c^{pl} = \varepsilon_c^{in} - \frac{d_c}{(1-d_c)}\frac{\sigma_c}{E_0} \tag{6}$$

When concrete is subjected to uniaxial cyclic loading, its elastic stiffness partially recovers after the loading direction reverses. At this stage, it is assumed that the elastic modulus of the damaged concrete is represented by the undamaged elastic modulus $E_0$ and the stiffness degradation factor $d$, with the expression given as:

$$E = (1-d)E_0 \tag{7}$$

The accuracy of the damage factor in the concrete plastic damage model is one of the key factors influencing the computational reliability of the ballastless track–subgrade system model established in this study. To validate the reasonableness of the adopted concrete plastic damage parameters, standard cubic specimens of C60 and C40 grade concrete were modeled in ABAQUS. A displacement-controlled loading was applied to simulate their uniaxial compressive mechanical response.

Figure 3 presents the comparison between the simulated stress–strain curves and the theoretical results from the *Code for Design of Concrete Structures* (GB 50010-2010). The results show a good agreement, with the simulation error for uniaxial compression kept within 5%, thus confirming the accuracy and applicability of the selected concrete plastic damage model parameters used in this study.

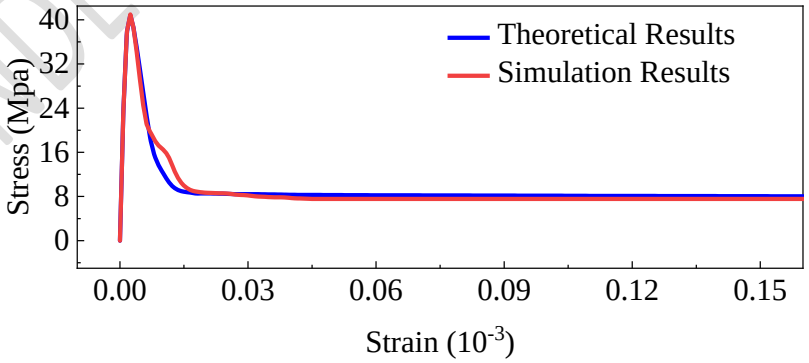


**Fig 3. Comparison between theoretical and simulation results**

### 1.2 *Validation of Frost Heave Curve*

Frost heave damage in subgrades exhibits randomness, uncertainty, and heterogeneity. Considering that vertical unevenness caused by frost heave is a particularly typical issue in

railway maintenance practice, this study temporarily neglects the influence of transverse frost heave non-uniformity and simplifies the longitudinal frost heave deformation along the track line into the following cosine function form:

$$y = \frac{f_0}{2}\left(1-\cos\left(\frac{2\pi(z-z_0)}{L}\right)\right) \tag{8}$$

Which, $L$ represents the frost heave wavelength; $Z_0$ denotes the frost heave starting position; $Z$ is the longitudinal coordinate; and $f_0$ is the frost heave amplitude, as illustrated in Fig. 4.

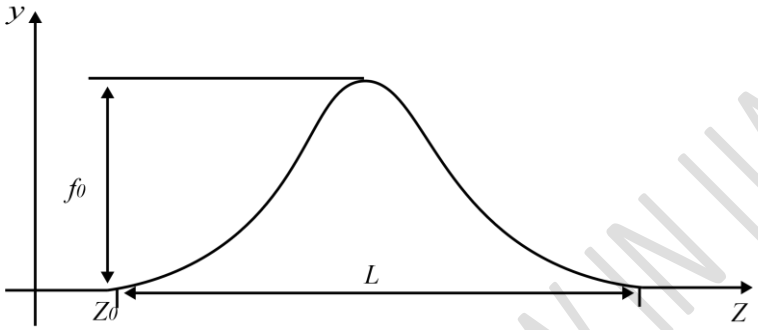


**Fig .4 Simplified cosine-shaped frost heave curve**

Figure 5 shows typical waveform segments extracted from the inspection data of the CRH380B train operating on the Harbin–Dalian High-Speed Railway.

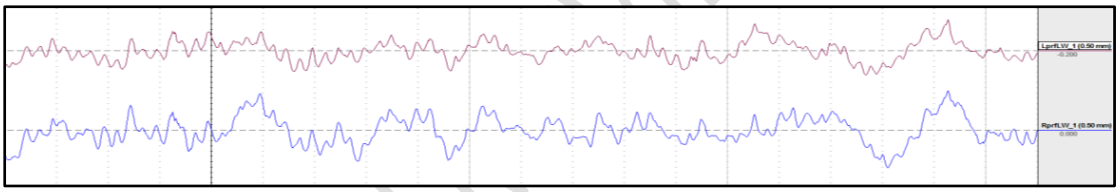

**Fig . 5 Measured frost heave deformation on Harbin–Dalian HSR**

The comparison in Figure 5 shows that the deformation trends along the left and right track measurement lines in the frost heave region are generally consistent, both exhibiting continuous multi-peak patterns. The waveform profiles closely approximate a cosine curve, indicating that the longitudinal frost heave deformation along the track demonstrates good periodicity and is well-suited for fitting.

## 2. Plastic Damage Model of Ballastless Track

### 2.1 *Ballastless Track Damage Model*

The CRTSI-type slab track is a layered composite structure, as illustrated in Figure 6. The top layer consists of WJ-7 type shoulderless fasteners securing the rails. The middle layer is composed of C60 precast concrete track slabs and a low elastic modulus CA mortar layer; the track slabs are internally reinforced with bidirectional prestressed steel bars and conventional steel mesh. The bottom layer is a cast-in-place C40 reinforced concrete base slab with bidirectional double-layer reinforcement, cast in segmented continuous pours, and connected between segments via expansion joints and shear keys. A 50 mm thick CA mortar layer is placed between the track slab and base slab to serve as a stress buffer. The ends of the track slabs feature cylindrical convex collars with a radius of 250 mm; this structure is cast integrally with the base slab, flush with the track slab surface, providing bidirectional

displacement restraint. To ensure structural continuity and integrity, this study adopts a consistent structural modeling approach for subgrade, bridge, and tunnel sections. Relevant modeling parameters are listed in Table 1.

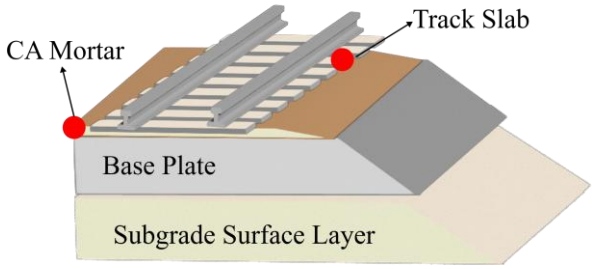


**Fig 6. Schematic diagram of the CRTSI ballastless track structure**

**Table 1 Modeling parameters of the ballastless track structure**

| Component | Parameter | Value | Unit |
|---|---|---|---|
| **Rail** | Elastic Modulus | 2.06×105 | MPa |
| | Poisson's Ratio | 0.3 | - |
| | Density | 7.8×103 | kg/m³ |
| **Fastener** | Spacing | 625 | mm |
| | Lateral Stiffness | $3\times10^4$ | N/mm |
| | Vertical Stiffness | $5\times10^4$ | N/mm |
| | Longitudinal Stiffness | $3\times10^4$ | N/mm |
| **Shoulder Block** | Elastic Modulus | $3.3\times10^4$ | MPa |
| | Poisson's Ratio | 0.2 | - |
| | Density | $2.5\times10^3$ | kg/m³ |
| **Track Slab** | Elastic Modulus | $3.6\times10^4$ | MPa |
| | Poisson's Ratio | 0.2 | - |
| | Density | $2.5\times10^3$ | kg/m³ |
| **CA Mortar** | Elastic Modulus | 300 | MPa |
| | Poisson's Ratio | 0.2 | - |
| | Density | $2.5\times10^3$ | kg/m³ |
| **Base Plate** | Poisson's Ratio | 0.2 | |
| | Elastic Modulus | $3.25\times10^4$ | MPa |
| **Subgrade** | Elastic Modulus | $1.8\times10^3$ | MPa |

## 2.2 *Interlayer Contact of Ballastless Track*

According to the relevant technical requirements of the *Code for Design of High-speed Railway* [10], the three-dimensional finite element model of the ballastless track established in this study adopts a differentiated simulation strategy for the contact relationships between structural layers, detailed as follows:

Between the subgrade and the base slab: normal “Hard Contact” and tangential Coulomb friction models are used, with a friction coefficient of 0.7 to reflect the actual shear resistance capability. Between the base slab and the track slab, and between the track slab and the CA

mortar: tie constraints are applied to ensure overall cooperative deformation among the multilayered structures. Between the track slab and the rail: a three-directional nonlinear spring-damper element simulates the connection behavior of the WJ-7 fastening system. This spring element features a compression-only constitutive behavior, and its stiffness parameters are calibrated based on field-measured data to enhance the engineering fidelity of the model response.

To verify the rationality and accuracy of the interlayer contact settings in the ballastless track model [11], a simplified frost heave deformation curve (wavelength L=10, amplitude $f_0$=10 mm） was applied at the bottom of the subgrade to simulate the deformation transfer process during frost heave. Theoretically, this frost heave displacement should be transmitted upward layer by layer to the track slab, demonstrating the interactive response characteristics of the multilayer “subgrade–base slab–track slab” system.

The vertical displacement variations of each structural layer (subgrade, base slab, track slab) obtained during the simulation are shown in Figure 7, further confirming the effectiveness and physical rationality of the model’s contact setting.

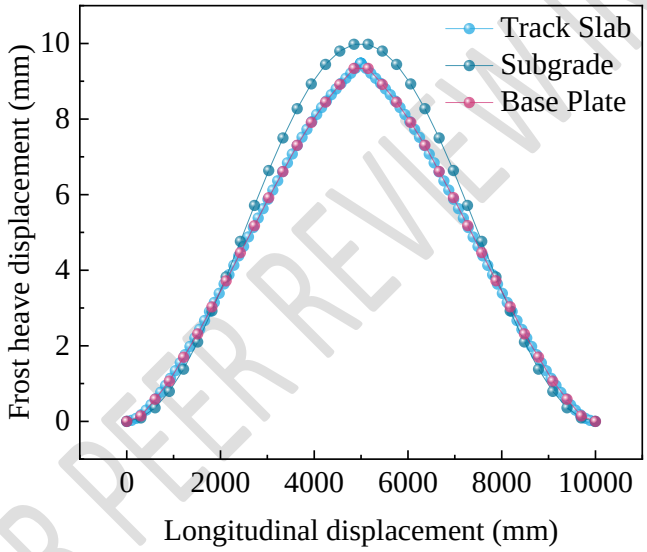


**Fig .7 Vertical displacement profiles of each layer**

## 3. Effects of Frost Heave Parameters

### 3.1 *Effects of Frost Heave Wavelength and Location*

In this study, two main frost heave locations within the subgrade are considered, as illustrated in Fig. 8. When the frost heave peak is located at the middle of the base slab, it is defined as position a; when the frost heave peak is located at one-quarter length of the base slab (corresponding to the middle of the track slab), it is defined as position b. The damage energy dissipation of the base slab and track slab throughout the entire process under each condition is analyzed.

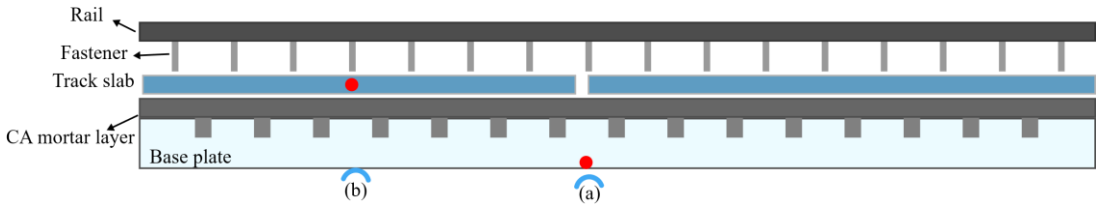

**Fig .8 Schematic diagram of frost heave locations**

The calculation results indicate that the damage to the track structure caused by subgrade frost heave is mainly concentrated near the frost heave wave peaks and the start and end points. Both the base slab and track slab surfaces, as well as the vicinity of the restraining structures, experience significant tensile stresses, making these areas prone to tensile damage. Compressive damage is minimal and can be neglected.

对其不同位置不同构件的损伤能进行统计如表 2 所示

**Table 2 Variation in damage energy of the two components**

| **Location a** | | |
|---|---|---|
| **Wavelength (m)** | Track Slab Damage Energy (KJ/m³) | Base Slab Damage Energy (KJ/m³) |
| **10** | 26.4 | 66.2 |
| **15** | 15.8 | 46.1 |
| **20** | 9.2 | 23.6 |

Additionally, this study investigates the variation of damage energy for the two components when the frost heave peak is located at position b, as shown in Table 3.

**Table 3 Variation in damage energy of the two components**

| **Location b** | | |
|---|---|---|
| **Wavelength (m)** | **Track Slab Damage Energy (KJ/m³)** | **Base Slab Damage Energy (KJ/m³)** |
| **10** | 31.2 | 79.8 |
| **15** | 20.5 | 51.3 |
| **20** | 12.1 | 28.3 |

From the two tables, it can be observed that when the frost heave peak shifts from position a to position b, the damage energy of both the track slab and base slab significantly increases. For example, at a wavelength of 15 m, the damage energy of the track slab and base slab increases by approximately 30% and 10.1%, respectively. This is mainly due to the more intense local coupling of tensile and compressive stresses inside the concrete when the frost heave peak is at position b, which accelerates damage evolution. The difference in the rate of damage energy increase between the two components is attributed to the base slab acting as a flexible support that can disperse part of the frost heave force through elastic deformation.

For the same wavelength of 10 meters, when the frost heave peak is located at position a, the track slab damage energy is 26.4 KJ/m³; when the frost heave peak is at position b, it increases to 31.2 KJ/m³, representing an 18% increase year-on-year. The detailed variation is shown in Fig. 9(a). Meanwhile, the base slab damage energy is 66.2 KJ/m³ at position a and rises to 79.8 KJ/m³ at position b, corresponding to a 20.5% year-on-year increase. The specific changes are illustrated in Fig. 9(b).

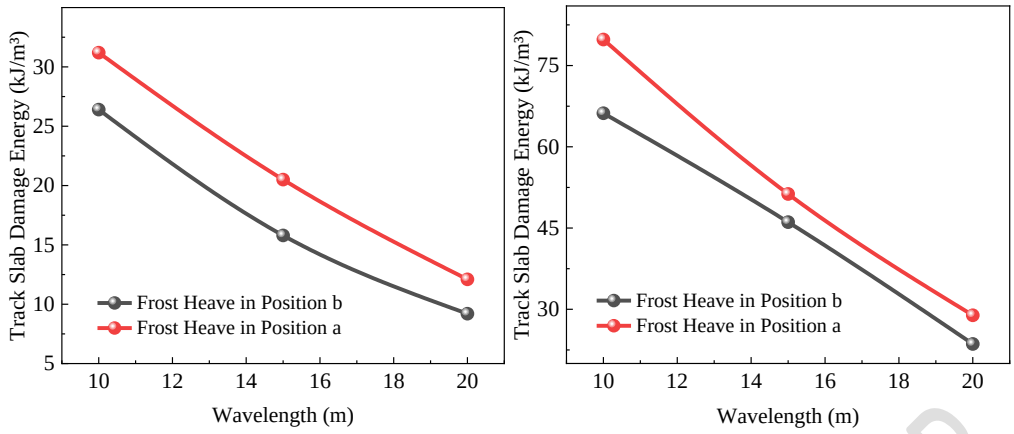


**Fig. 9 Damage energy variation of the two components with frost heave peak position ;(a) Variation of track slab damage energy with different frost heave peak positions; (b) Variation of base slab damage energy with different frost heave peak positions**

Based on operational practices from the Harbin–Dalian High-Speed Railway and others, vertical deformation amplitudes caused by frost heave in the subgrade are distributed as follows: 0–5 mm accounts for 73.91%, 5–10 mm for 21.9%, 10–15 mm for 3.7%, and above 15 mm for 0.49%. To better reflect the influence of wavelength on the damage energy of the two components, wavelengths of 10, 15, and 20 meters were selected for the study.

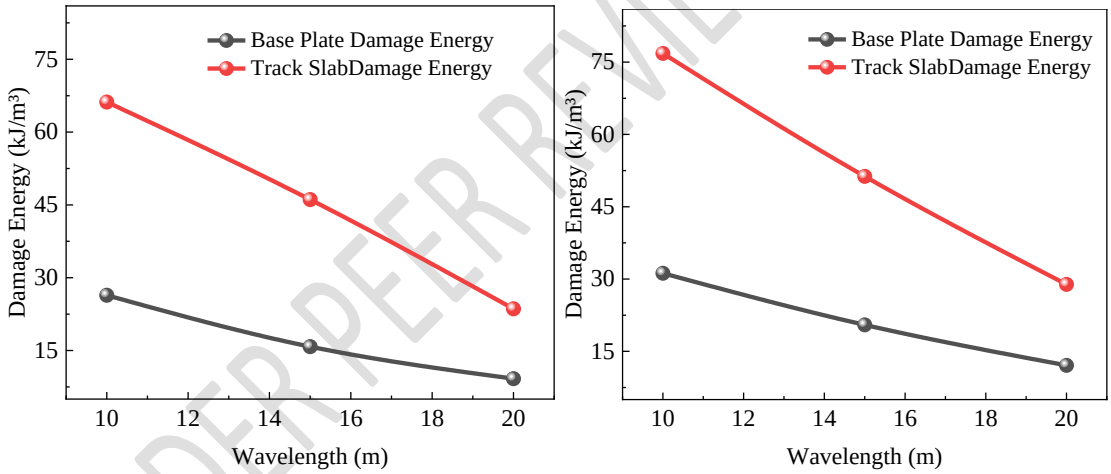


(a) Damage Energy Variation at Position a (b) Damage Energy Variation at Position b

**Fig. 10 Damage energy variation of the two components**

As shown in Fig. 10, the damage energy of both components decreases with increasing frost heave wavelength, and the rate of decline gradually slows. This trend is primarily due to the smoother deformation profile associated with longer wavelengths, which significantly reduces the stress gradient within the track slab and thus suppresses damage propagation. In contrast, shorter wavelengths correspond to high-frequency deformation, which tends to induce stress concentration at the interface between the track slab and the base slab, leading to local debonding or cracking and accelerating damage accumulation.

It is worth noting that the damage energy of the two components exhibits distinct patterns. The damage energy of the base slab shows an approximately linear negative correlation with wavelength and a relatively smaller decline rate. This behavior is mainly attributed to the excellent deformation compatibility of the base slab as a large structural

component, which enables better adaptability to long-wavelength frost heave deformation.

### 3.2 *Influence of Frost Heave Amplitude*

Taking a short-wavelength frost heave case with a wavelength of 10 m, peak position at location a, and amplitude ranging from 0 to 20 mm as an example, different frost heave amplitudes are used to clearly illustrate the evolution of the track slab and base slab across the three stages of concrete plastic damage: elastic stage, micro-damage stage, and macroscopic cracking stage.

Due to its lower strength and direct exposure to frost heave loads, the base slab exhibits more pronounced damage progression—particularly in compressive zones—where it is more prone to entering the failure stage. This process manifests as micro-damage initiation under low amplitude, damage accumulation and expansion under medium amplitude, and macroscopic crushing under high amplitude.

Given this characteristic, the base slab requires more attention during maintenance and is thus more suitable than the track slab as a subject of study. Therefore, damage factor contour plots for the base slab under amplitudes of 4 mm, 6 mm, and 20 mm are presented in Fig. 11.

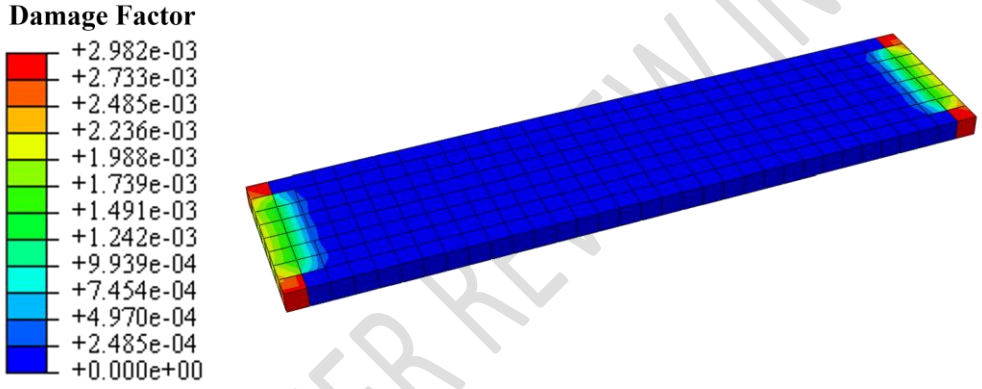


(a) Damage contour of base slab under 4 mm frost heave amplitude

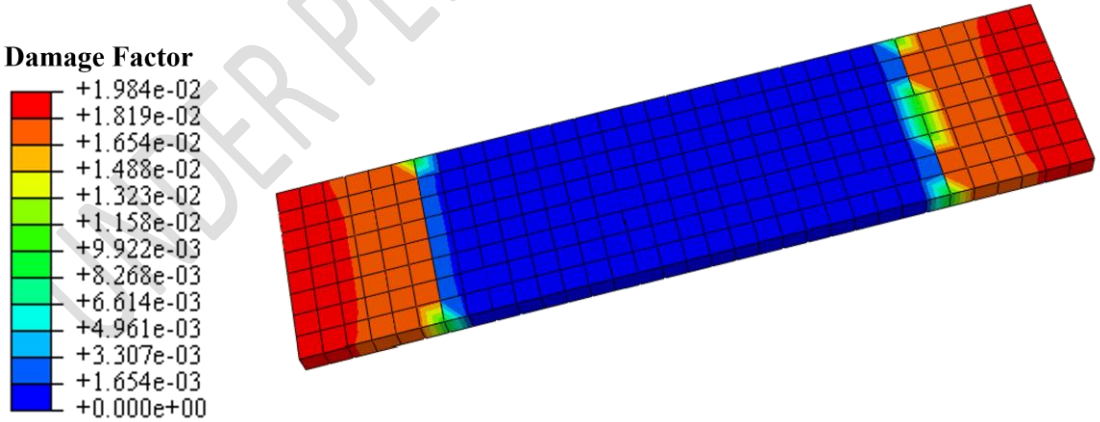


(b) Damage contour of base slab under 6 mm frost heave amplitude

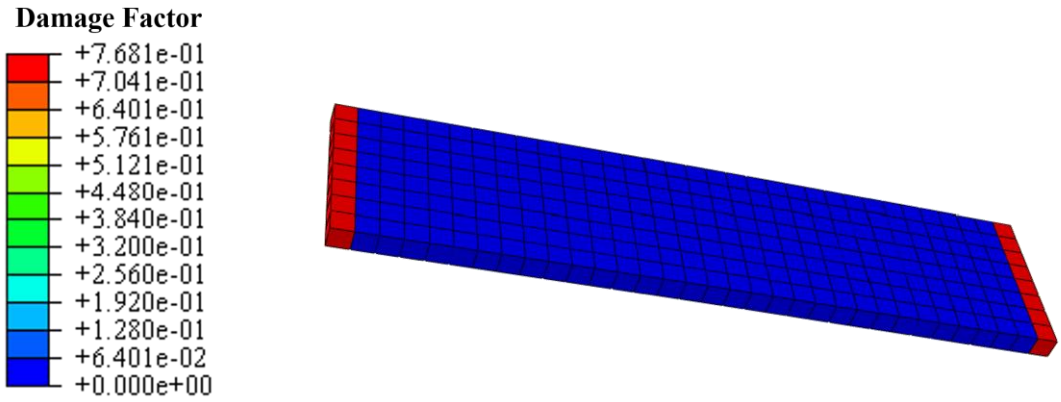


(c) Damage contour of base slab under 20 mm frost heave amplitude

**Fig .11 Damage contour plots**

As shown in Fig. 12, under a constant frost heave wavelength, the maximum principal tensile stress in both the track slab and base slab initially increases with rising frost heave amplitude. The tensile stress in the base slab increases more rapidly and tends to stabilize after exceeding the tensile strength of concrete.

Before reaching strength failure, the rapid increase in tensile stress within the base slab may be attributed to its short longitudinal continuity and strong interlayer constraints.

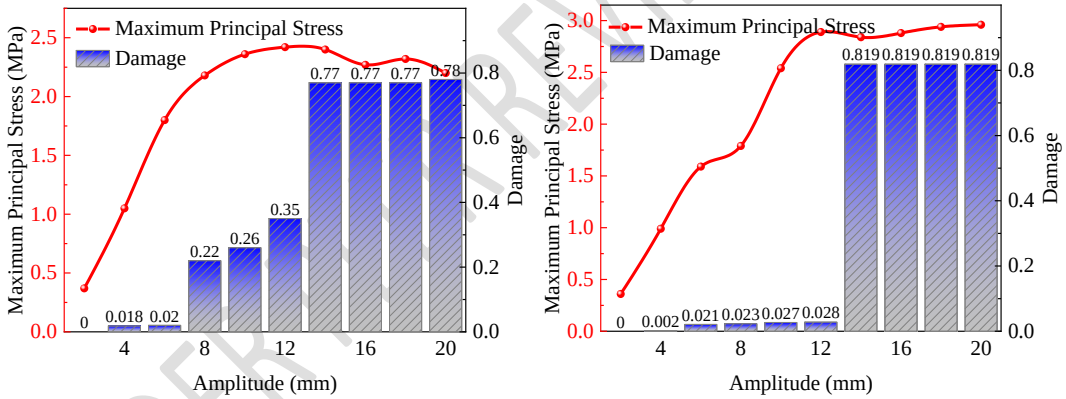


(a) Base slab (b) Track slab

**Fig .12 Comparison of maximum principal stress and damage distribution of two components under frost heave conditions (amplitude-dependent)**

### 3.3 *Relationship Between Frost Heave Amplitude and Damage Factor*

As shown in Fig. 12, under a frost heave wavelength of 10 m, the damage evolution of both the track slab and base slab exhibits a clear three-stage behavior:

Elastic Stage: At this stage, the damage factor for both components is zero, and the stress–strain relationship remains linear. The maximum principal stress of the base slab increases from 0.37 MPa to 1.05 MPa, and that of the track slab rises from 0.36 MPa to 0.99 MPa, both remaining below the tensile strength of the material. Micro-Damage Stage: At an amplitude of 8 mm, the damage factor of the base slab sharply increases to 0.22, indicating localized plastic deformation. In contrast, the track slab exhibits a delayed damage response, with a damage factor of only 0.028 at the same amplitude. This reflects differing behaviors between the two components in this stage.

Macroscopic Failure Stage: The damage factor of the base slab rises rapidly to the range of 0.35–0.78, accompanied by a slight decrease in principal stress, signifying the development of crushed zones. For the track slab, the damage factor surges to 0.819, while the principal stress remains high (2.84–2.96 MPa), indicating residual tensile strength following crack penetration.

Based on the damage evolution, the damage process of the ballastless track system can be categorized into three stages: Stage I (Damage Factor 0–0.25): Microcrack initiation. The track structure gradually transitions into an elastoplastic state, with initial stiffness degradation and the onset of damage. Stage II (Damage Factor 0.3–0.8): Rapid propagation of microcracks. Macroscopic cracks appear, and plastic characteristics become pronounced. Stage III (Damage Factor 0.8–1): Secondary cracking and damage localization. Well-defined damage zones emerge. The frost heave amplitudes corresponding to each stage for both components under a 10 m wavelength are summarized in Table 4.

**Table 4 Frost heave amplitude characteristics corresponding to each damage stage under a 10 m wavelength**

| Component | Elastic Stage | Stage I | Stage II | Stage III |
|---|---|---|---|---|
| **Track Slab** | 0~4.5mm | 4.5~8.8mm | 8.8~13mm | ＞13mm |
| **Base Slab** | 0~4mm | 4~8.5mm | 8.5~12mm | ＞12mm |

As shown in the table, during the damage evolution process, the base slab exhibits significantly faster damage progression compared to the track slab. This is primarily due to several factors:

First, there is a difference in material strength between the two components—the base slab has a lower tensile strength than the track slab, causing it to reach the yield threshold earlier under the same frost heave amplitude [12]. Second, due to differences in load transfer mechanisms, the frost heave load is directly applied to the base slab in the designed scenario, resulting in the compression zone of the base slab entering the plastic stage earlier. In contrast, the track slab experiences tensile stress indirectly through deformation of the base slab, leading to slower damage accumulation. Lastly, the two components exhibit different failure modes: the base slab primarily undergoes compressive softening [13] (evidenced by a decline in principal stress after reaching the peak), whereas the track slab shows tensile ductility (principal stress remains high), highlighting the decisive influence of concrete strength grade on damage evolution.

Therefore, in the maintenance of CRTS I slab track systems, priority should be given to monitoring and mitigating the risk of base slab crushing [14], while long-term monitoring should also be conducted on tensile cracking in the track slab to prevent progressive deterioration.

## 4 Conclusions

1. Differences in Damage Evolution Timing

The base slab enters a significant damage stage at a frost heave amplitude of 8.5 mm (damage factor = 0.25), while the track slab does not exhibit a sudden increase in damage until an amplitude of 13 mm (damage factor = 0.819). This indicates that, due to its lower strength, the base slab experiences earlier damage initiation and faster progression compared to the track slab.

2.Comparison of Failure Modes

The base slab primarily undergoes compressive softening, as evidenced by a drop in principal stress (from 2.4 MPa to 2.2 MPa) when the damage factor reaches 0.78, reflecting localized crushing. In contrast, the track slab exhibits tensile ductility; even after a sharp increase in the damage factor, the principal stress remains high (2.96 MPa), indicating a residual load-bearing capacity after crack penetration.

3.Maintenance Priority Recommendations

For frost heave amplitudes ≥ 8 mm, attention should be focused on the compressive damage in the base slab to prevent progressive crushing. When the amplitude reaches ≥ 13 mm, the tensile cracking in the track slab should be monitored to avoid fatigue accumulation. These differences imply that maintenance strategies must be component-specific, with priority given to ensuring the structural integrity of the base slab.

## References


[1] Yu, C., Zhang, W., Wang, X., & Li, C. (2018). Influence of slab arch imperfection of double-block ballastless track system on vibration response of high-speed train. *Journal of the Brazilian Society of Mechanical Sciences and Engineering, 40*, 1–14. https://doi.org/10.1007/s40430-018-1175-6.

[2] Xu, H., Cai, W., & Wang, P. (2019). Research on the influence of subgrade frost heave on CRTSIII slab ballastless track. *Journal of Railway Engineering Society, 36*(10), 27–32, 40. *(In Chinese)*.

[3] Wang, B., Wang, F., & Wang, Q. (2018). Damage constitutive models of concrete under the coupling action of freeze–thaw cycles and load based on Lemaitre assumption. *Construction and Building Materials, 173*, 332–341. https://doi.org/10.1016/j.conbuildmat.2018.03.262.

[4] Wang, H., Xiao, H., Cui, X., Yang, S., Nadakatti, M. M., & Guo, Q. (2023). Influence of uneven subgrade frost heave on deformation and damage of CRTSIII slab track. *Applied Sciences, 13*(9), 5345. https://doi.org/10.3390/app13095345 .

[5] Zeng, Z., Peng, G., Wang, W., Huang, X., Shen, S., Shuaibu, A. A., & Meng, X. (2022). Research on the variable-temperature cracking mechanism of CRTS I type double-block ballastless track on a bridge. *Materials, 15*(3), 770. https://doi.org/10.3390/ma15030770.

[6] Song, L., Liu, H., Xu, L., Wang, C., & Zhang, Y. (2023). Dynamic performance of CRTS III ballastless track structure under the train load and temperature. In *Structures* (Vol. 53, pp. 408–420). Elsevier. https://doi.org/10.1016/j.istruc.2023.01.066.

[7] Ministry of Housing and Urban-Rural Development of the People's Republic of China. (2010). Code for design of concrete structures (GB 50010-2010). Beijing: China Architecture & Building Press. (*In Chinese*).

[8] Cui, X. (2022). Influence of uneven subgrade settlement on dynamic characteristics and damage behavior of CRTS II slab ballastless track (Master's thesis, Beijing Jiaotong University). https://doi.org/10.26944/d.cnki.gbfju.2022.000240 (In Chinese).

[9] Jing, P., Xiao, J., Zhuang, L., Zhang, H., & Li, Y. (2021). Study on nonlinear damage mechanism of CRTSIII slab ballastless track in seasonally frozen areas. Journal of Railway Science and Engineering, 18(7), 1686–1695. https://doi.org/10.19713/j.cnki.43-1423/u.t20200873 (*In Chinese*).

[10] National Railway Administration of the People's Republic of China. (2014). Code for design of high-speed railway (TB 10621-2014). Beijing: China Railway Publishing House. (*In Chinese*).

[11] Deng, Z., Xie, K., Wang, W., & Zhang, H. (2025). Research on evaluation method and application of dynamic stability performance of high-speed railway subgrade. Journal of the China Railway Society, 47(3), 126–134. (*In Chinese*).

[12] Cai, X., Liang, Y., Tan, S., & Shen, Y. (2017). Deformation and seam characteristics analysis of CRTSI slab ballastless track in subgrade frost heaving zone. *Journal of Beijing Jiaotong University, 41*(1), 7–13. *(In Chinese)*.

[13] Li, Y., Guo, H., Zhou, H., Yang, Y., & Zhang, Y. (2022). Damage characteristics and constitutive model of concrete under uniaxial compression after freeze–thaw damage. Construction and Building Materials, 345, 128171. https://doi.org/10.1016/j.conbuildmat.2022.128171.

[14] Zhao, G., Liu, J., Li, M., & Xu, D. (2018). Study on damage control standard of CRTS I ballastless track subgrade under frost heave. China Railway Science, 39(3), 1–9. (*In Chinese*)